Progress In Electromagnetics Research B, Vol. 99, 139–157, 2023

Dual-Band Hexagonal SRR Antennas and Their Applications in SIMO and MISO-Based WLAN/WiMAX Systems

Puneet Sehgal[1, 2] and Kamlesh Patel[2, *]

Abstract—This article presents the performance of a hexagonal split-ring resonator (H-SRR) antenna in the 2.4/5.2 GHz bands and evaluation of channel capacity for single-input multiple-output (SIMO) and multiple-input single-output (MISO) systems. The proposed antenna consists of two hexagonal-shaped split-ring resonators for dual-band operation with higher gain and metallic loadings between the rings to achieve a wide impedance bandwidth. Impedance modeling of the proposed antennas confirms the role of conductance and inductance of metallic loading for enhancing the antenna characteristics, and thus, the fabricated H-SRR antenna achieves dual-band features with improved impedance bandwidth of 50%/76% and a gain of 2.32/2.57 dB at 2.4/5.2 GHz frequency bands. The performance of the hexagonal SRR antenna is then investigated for space diversity applications in the 1×3 SIMO and 3×1 MISO systems with circular SRR antennas. In linear and spherical arrangements of the antennas, the channel capacity is found in the range of 2.7 to 4.8 Mbps at the 2.4/5.2 GHz bands, which also confirms its dependency on the number of antennas as well as on the placement of antennas.

1. INTRODUCTION

New wireless applications demand ever-increasing data rates from both cellular and non-cellular networks, like in technologies for robots, drones, self-driving vehicles, and new medical devices. To satisfy these requirements in non-cellular networks, the wireless local area network (WLAN) standard is continually being extended for a noise-free, disturbance-free effective communication channel with minimum data loss, and a good value of signal-to-noise ratio (S/N) for reliable transmission of data [1]. So, two features, namely wide bandwidth and high channel capacity, of such networks can help to achieve the future demand for more channels with high transmission speed. To increase it, various system configurations based on the number of transmitting and receiving antennas are proposed, namely, single-input single-output (SISO), single-input multiple-output (SIMO), and multiple-input single-output (MISO), and multiple-input multiple-output (MIMO) [2].

The channel capacity of these systems depends upon the bandwidth of transmission and the S/N ratio in addition to the characteristics of antennas used. In these four configurations, the channel capacity (CC) is around 1 bps/Hz for a 1×1 SISO system [3–6], 1 to 3.4 bps/Hz for a 1×4 SIMO system [6], and 1 bps/Hz for 4×1 MISO system even though 10 transmitting antennas are used [2, 6], whereas in MIMO, where multiple antennas are used at the transmitter end as well as at the receiver end, CC is reported to increase to 1 to 8.3 bps/Hz for 4×4 MIMO system for 10 transmitting antennas [6–8]. However, the major drawbacks of the MIMO system are mutual coupling and large size. In MIMO systems, the use of space diversity makes channel communication more effective by minimizing the effects of multipath fading [9]. The selection of a suitable system configuration depends on the fading

Received 15 December 2022, Accepted 18 March 2023, Scheduled 2 April 2023

* Corresponding author: Kamlesh Patel (kpatel@south.du.ac.in).

[1] Atma Ram Sanatan Dharma College, University of Delhi, Dhaula Kuan, New Delhi 110021, India. [2] Department of Electronic Science, University of Delhi South Campus, New Delhi 110021, India.

level between one element and another in a network [10] like in urban areas and also on several multi-path components which add up differently with each element, and their independent fading develops easily [11]. So, as in space diversity, the wireless or RF paths are used to place the antennas at least one-half wavelength or several wavelengths apart at the source (transmitter diversity) or receiving ends (receiver diversity), or both [12, 13]. For ultra-wideband (UWB) applications, planar monopole antennas are preferred due to their simple small structure, wide impedance bandwidth, and good omnidirectional radiation patterns [14]. For WLAN (2.4/5.2 GHz)/WiMAX (3.4 GHz) applications [15], the interest in split-ring resonator (SRR)-based antennas is growing as this structure offers miniature size with resonant behavior [16, 17]. Such antennas are usually fed by coplanar waveguide (CPW) lines for better impedance matching [17–19]. Different shapes of SRR antennas have been investigated in WLAN/WiMAX applications previously, like rectangular, circular [20, 21], and hexagonal SRRs [22–25]. These antennas were reported with a gain range of 2.32/2.57 dB and an impedance bandwidth range of 27.67/74.50% in 2.4/5.2 GHz bands. For various WLAN/WiMAX applications, the channel capacity desires various factors like high-efficiency antennas, low interference of signals, and the minimum effect of multi-path propagation which are quite prevalent nowadays in the technological era of wireless communication [26]. Before employing SRR-based antenna into a MIMO system independently or on the same substrate, first, the performance of these antennas is required to be investigated in a simpler systems like SIMO and MISO. There are very few reports available on such investigation in WLAN/WiMAX applications in 2.4/5.2 GHz bands.

In this paper, a hexagonal split ring resonator (H-SRR) structure with coplanar waveguide transmission (CPW) feed is proposed as a compact wideband monopole antenna and first optimized in ANSYS High-Frequency Structure Simulator (HFSS) software on an FR-4 substrate along with different metallic loadings. The simulated results are then compared with a circular SRR antenna (C-SRR) [21], and the optimized H-SRR antenna is fabricated on an FR-4 substrate. The space diversity performance is investigated by employing two H-SRR and two C-SRR antennas for the receiver diversity (SIMO system) and transmitter diversity (MISO system) in two arrangements of antennas, linear and spherical. The channel capacity of these systems is evaluated at a low bandwidth of 10 kHz to explore the future possibility of using H-SRR antennas in dual-band operation for SIMO/MISO communication systems.

2. DESIGN OF HEXAGONAL SRR ANTENNA

The dimensions of proposed antenna are calculated using the design equations reported earlier [21]. An equivalent circuit model of the H-SRR antenna is shown in Figure 1, where L_1, C_1 represent the outer ring, corresponding to a lower resonating frequency of 2.4 GHz, and L_2, C_2 represent the inner ring with an upper resonating frequency of 5.2 GHz. Thus, it acts as an L-C tank circuit that operates at a particular resonance frequency for a single ring of SRR.

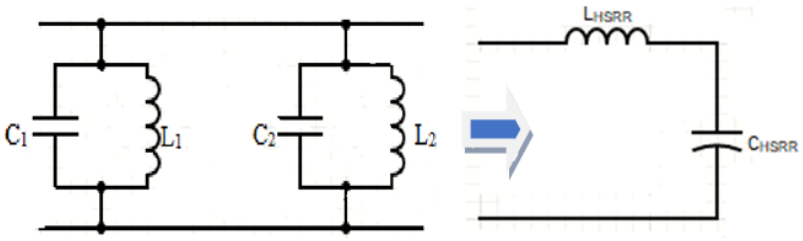

Figure 1. Equivalent circuit of H-SRR structure.

The inductance of the tank circuit ($L_{\text{H-SRR}}$) is calculated using Equation (1) [27]

$$L_{\text{H-SRR}} = \frac{\mu_0}{2}\left[x - (N-1)(t+s)\right] 4.86 \left[\ln\frac{0.98}{\alpha} + 1.84\alpha\right] \quad (1)$$

where α is the fill ratio as defined in Equation (2), μ_0 the permeability of free space, 'N' the number of rings in the SRR structure, 't' the strip width of SRR rings, and 's' the spacing between the SRR

rings. Here, α is defined as [27],

$$\alpha = \frac{(N-1)(s+t)}{1-(N-1)(s+t)} \tag{2}$$

The equivalent capacitance of the hexagonal SRR structure ($C_{\mathrm{H-SRR}}$) is obtained using Equation (3) [27].

$$C_{\mathrm{H-SRR}} = \frac{(N-1)}{2}\left[2x-(2N-1)(t+s)\right]\varepsilon_0\frac{(1+\varepsilon_0)}{2}\frac{\varepsilon(\sqrt{1-\sigma^2})}{\varepsilon(\sigma)} \tag{3}$$

where x is the length of the outermost ring, ε_0 the permittivity of the free space, $\varepsilon(\sigma)$ the complete integration of the first kind, $\varepsilon(\sqrt{1-\sigma^2})$ the complete integration of the second kind, and the value of σ (a constant) is obtained by $s/(s+2t)$ [27]. The resonance frequency is obtained by $f_r = \frac{1}{2\pi\sqrt{L_{\mathrm{H-SRR}}C_{\mathrm{H-SRR}}}}$. The dimensions of both rings of the H-SRR structure are shown in Table 1 along with calculated lumped components.

Table 1. Calculated set of physical parameters and resonant frequency of H-SRR antenna.

Various parameters	**Outer Ring**	**Inner Ring**
x (mm)	10	7
t (mm)	2.5	2.5
S (mm)	0.5	0.5
$\varepsilon(\sigma)$	89.82	89.82
$\varepsilon(\sqrt{1-\sigma^2})$	60	60
$C_{\mathrm{H-SRR}}$ (fF)	87.78	40
$L_{\mathrm{H-SRR}}$ (nH)	34.61	20.27
f_r (GHz) — calculated	2.6	5.4
f_r (GHz) — targeted	2.4	5.2

From Table 1, since there is a difference between the calculated and targeted resonance frequencies based on Equations (1) and (3), a few modifications are required to obtain the desired frequencies as well as to incorporate the effect of the feeding line, which is a tedious task. A solution can be found by properly optimizing the dimensions of the designed antenna by simulation. So, first, the H-SRR antenna design is made on ANSYS HFSS and then optimized to get a response at the desired frequencies as shown in Figure 2(a), where a coplanar waveguide (CPW) fed H-SRR antenna consists of two split-ring resonators in a hexagonal shape with outer radius ($R_1 = 7.5\,\mathrm{mm}$) and inner radius ($R_2 = 5.5\,\mathrm{mm}$), and the thickness of the hexagonal shape ring is '$t = 2.5\,\mathrm{mm}$'. The spacing between the two rings is '$s = 0.5\,\mathrm{mm}$'. Also, the dimensions $L_1 = 43\,\mathrm{mm}$, L_3 (length of the ground planes), $L_2 = 26\,\mathrm{mm}$ (breadth of antenna structure), the gap within both rings ($g = 1\,\mathrm{mm}$), $W_1 = W_3 = 11\,\mathrm{mm}$ (widths of top grounds), and $W_2 = 3\,\mathrm{mm}$ (width of the center CPW line) are taken the same as for the C-SRR antenna in [21]. S_1, S_2, S_3, and S_4 are the metallic loadings used for different designs in Figure 2(b) to achieve a wider bandwidth with good gain, and their dimensions are given in Table 2. All the antenna designs are made of the same size, i.e., $43 \times 26 \times 1.5\,\mathrm{mm}^3$. The H-SRR antenna is fabricated on FR-4 ($\varepsilon_r = 4.4$, $h = 1.5\,\mathrm{mm}$, loss tangent = 0.02 and 35 µm thick copper layer) for verification.

2.1. Return Loss and Gain Performance of the H-SRR Antenna

In this section, the simulated and measured return loss and gain characteristics of three proposed H-SRR designs, fabricated C-SRR [21] and H-SRR antennas are presented. As shown in Figure 3(a) compared to design 1 and design 2, design 3 of the H-SRR antenna gives better matching at higher impedance bandwidth (IBW) of 74.50% at 5.2 GHz while at lower band, i.e., 2.4 GHz, the IBW is

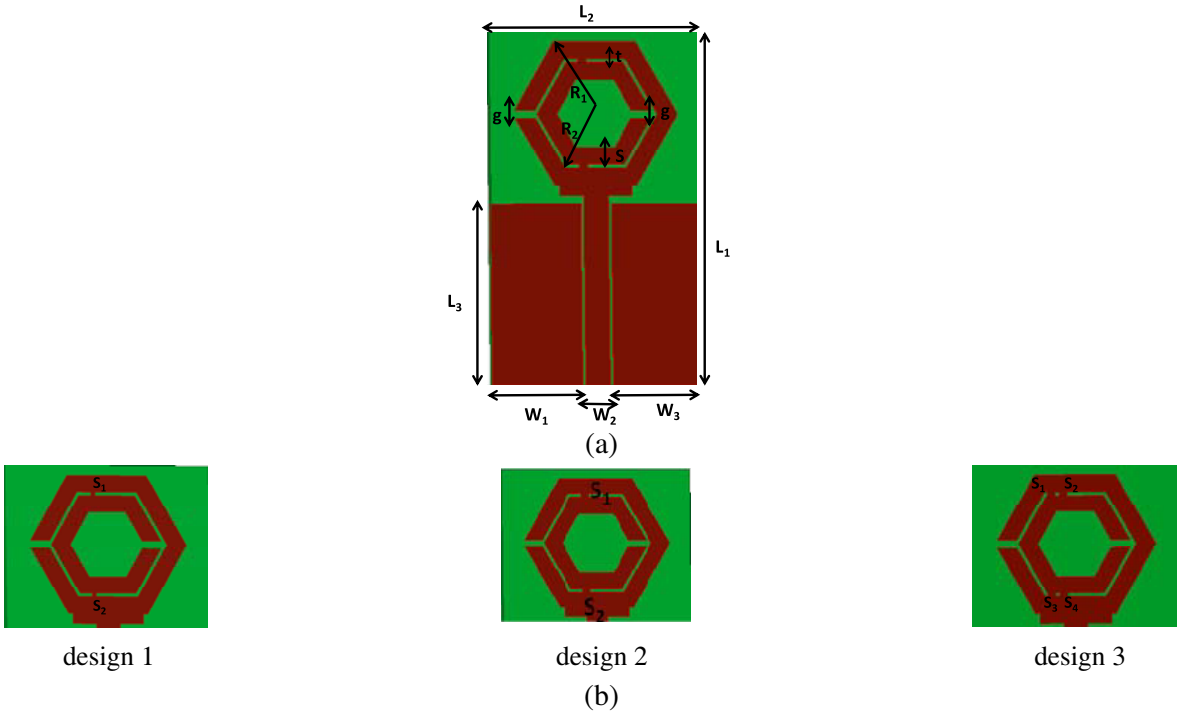

Figure 2. Schematics of (a) H-SRR antenna, (b) design 1, design 2, and design 3 with proposed modifications in position and numbers of metallic loadings, respectively.

Table 2. Size of metallic loadings for three H-SRR antenna designs.

Proposed designs	**Size of Metallic loadings (in mm^2)**
design 1	$S_1 = S_2 = 1.5 \times 0.5$
design 2	$S_1 = S_2 = 1.5 \times 1$
design 3	$S_1 = S_2 = S_3 = S_4 = 1.5 \times 1$

obtained as 27.67%. It is observed that with increasing width of metallic loading, return loss remains almost the same for design 1 and design 2. However, with adding one more metallic loading in design 3, a new current path led to a slightly extended higher-end frequency in both 2.4 GHz and 5.2 GHz bands, and the peaks in return loss shifted towards higher frequencies in Figure 3(a), which confirmed a minor decrease in the equivalent inductance due to mutual coupling of loadings. Also, as given in Figure 3(b), similar gains of 2.21 dB and 1.02 dB at 2.4 GHz and 5.2 GHz are obtained, respectively for all designs. Design 3 is selected for the fabrication for a comparatively wider bandwidth. Figure 3(c) and Figure 3(d) represent the measurement setup for the return loss and gain measurement using the R&S Vector Network Analyzer (VNA) model ZVH8 in an anechoic chamber. The discrepancy in measured and simulated results in Figure 3(e) is due to the fabrication tolerances and some variations in the actual substrate specifications compared to the simulated antenna.

The pairs of C-SRR and H-SRR antennas are taken, and their S-parameters are measured after the calibration of VNA and used to calculate the gain of the antenna using Equation (4) [28, 29].

$$G^2 = |S_{21}|^2 \Big/ \left\{ \left(1 - |S_{11}|^2\right) \left(1 - |S_{22}|^2\right) \left(\frac{\lambda}{4\pi r}\right)^2 E_P \right\} \tag{4}$$

where r is the distance between the antennas (here $r = 30$ cm); λ is the wavelength; G is the gain of the antennas (considered the same for identical antennas); S_{21}, S_{11}, S_{22} are the S-parameters; and E_P is the

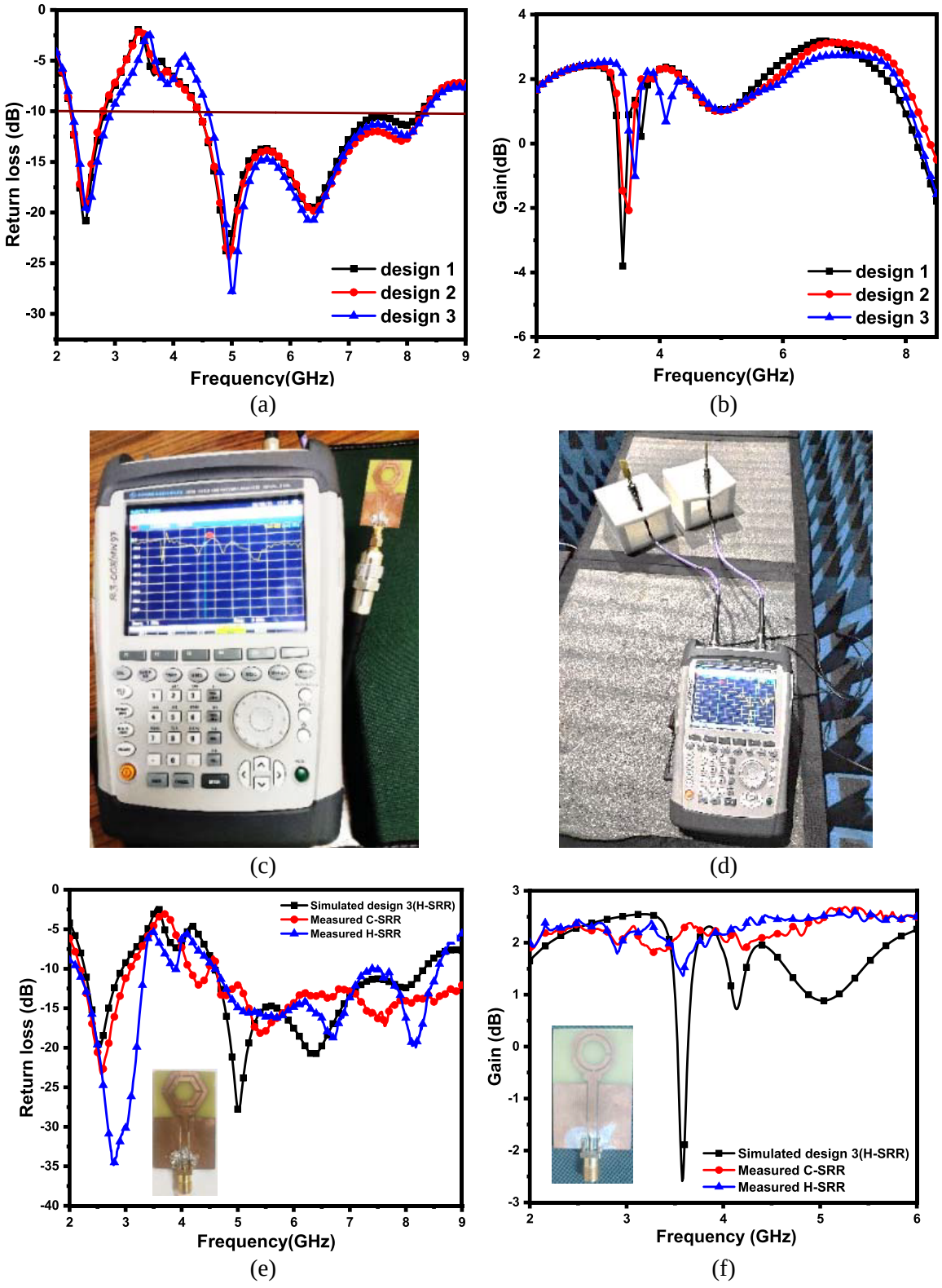

Figure 3. (a) Simulated return loss and (b) simulated gain response of design 1, design 2, and design 3, (c) return loss, and (d) gain measurement set up with R&S VNA ZVH8, (e) return loss comparison, and (f) gain comparison of simulated design 3, fabricated C-SRR, and fabricated H-SRR antennas.

Table 3. Comparison of antenna parameters of simulated and fabricated antennas.

Bands (GHz)	Parameters	design 1	design 2	design 3	C-SRR Antenna (Fabricated)	H-SRR antenna (Fabricated)
2.4	Return loss (dB)	−17.53	−17.14	−15.20	−17.71 @ 2.415 GHz	−18.55 @ 2.42 GHz
	Impedance Bandwidth (%)	24.34	23.90	27.67	36.85	**50**
	Gain (dB)	2.19	2.21	2.21	2.29	**2.32**
5.2	Return loss (dB)	−16.27	−16.36	−19.40	−15.67 @ 5.23 GHz	−15.60 @ 5.23 GHz
	Impedance Bandwidth (%)	72.62	74.42	74.50	83.75	**76.53**
	Gain (dB)	1.39	1.10	1.02	2.61	**2.57**

polarization efficiency (= 1 for co-polarized antennas). Figure 3(f) shows the simulated and measured gains of the H-SRR antenna (design 3). The measured gain of the C-SRR antenna is 2.29/2.61 dB at 2.415/5.23 GHz, and for the H-SRR antenna, it is obtained as 2.32/2.57 dB at 2.42/5.23 GHz. So, slightly better return loss and gain performances are obtained for fabricated H-SRR antenna than for C-SRR antenna as summarized in Table 3.

2.2. Radiation Characteristics Measurements

Figures 4(a)–(b) show the 3-D polar plots or far-field patterns to understand the directional properties of the H-SRR antenna (design 3) at frequencies 2.4/5.2 GHz. The maximum gain obtained is 2.3/3.67 dB at 2.4/5.2 GHz in these 3-D patterns. The pattern is almost omnidirectional at 2.4 GHz and radiates from both sides equally, whereas the radiation concentrates over the CPW feed line at 5.2 GHz rather than over the entire SRR area.

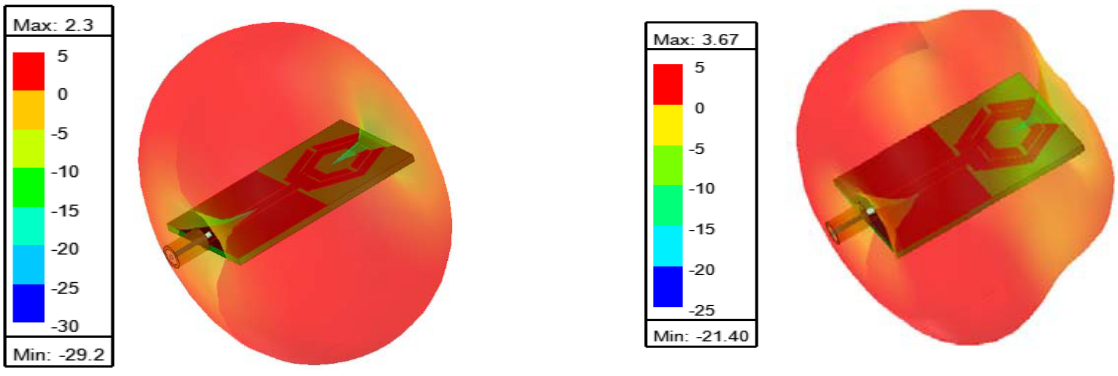

(a) (b)

Figure 4. 3-D polar plot of H-SRR antenna at (a) 2.4 GHz and (b) 5.2 GHz.

The 2-D radiation pattern of the proposed H-SRR antenna is measured using RIGOL signal generator model DSG3060 (9 kHz–6 GHz) and the ROHDE & SCHWARZ spectrum analyzer model FSL6 (9 kHz–6 GHz) in an anechoic chamber. Figures 5(a)–(d) show the simulated and measured 2-D radiation patterns of the proposed H-SRR antenna for E-plane (X-Z) and H-plane (X-Y) at 2.4/5.2 GHz frequencies, respectively. The omnidirectional pattern is obtained for H-plane, which is

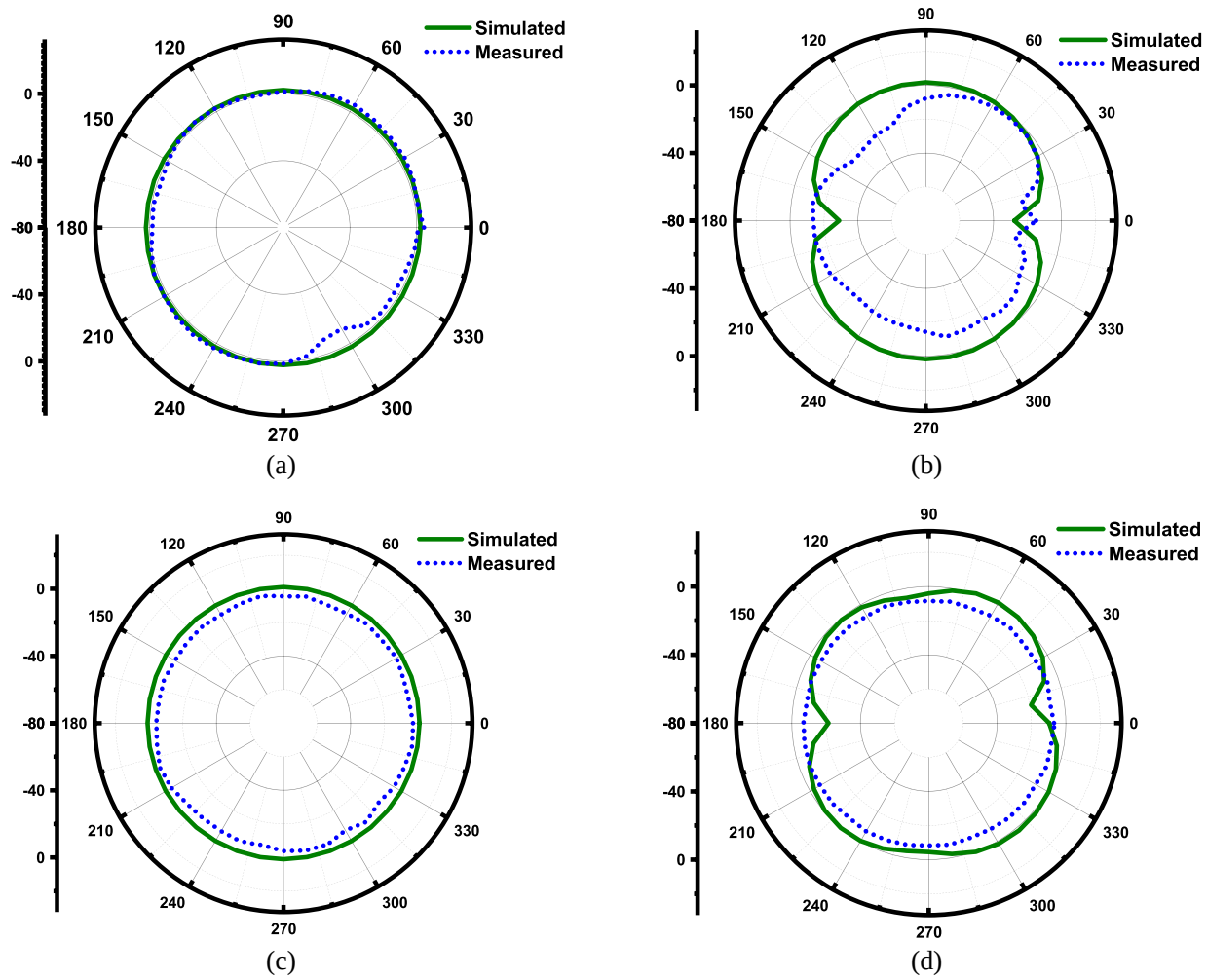

Figure 5. 2-D radiation patterns of H-SRR antenna (design 3) for (a) H-plane at 2.4 GHz, (b) E-plane at 2.4 GHz, (c) H-plane at 5.2 GHz, (d) E-plane at 5.2 GHz.

useful for applications like airplane antennas [20], while a dumbbell-shaped pattern is obtained for the E-plane, so this H-SRR antenna is promising for WLAN/WiMAX bands.

To understand the radiation mechanism, the current distribution mechanism of this antenna is investigated. The simulated surface current distributions are shown in Figures 6(a)–(b) at resonant frequencies, 2.4 GHz and 5.2 GHz. At 2.4 GHz, maximum radiation is contributed by the inner ring of the SRR structure and the central conductor of the CPW feed, while at 5.2 GHz the outer ring of the SRR structure and the central feed part contribute to the maximum radiation. The surface current density is obtained of the order of 39.6784 A/m at 2.4 GHz and 52.86 A/m at 5.2 GHz on the H-SRR antenna at different parts on its surface as shown in Figures 6(a)–(b), so the radiation occurs from the overall surface of rings leading to wider bandwidth due to four metallic loadings (S_1, S_2, S_3, S_4). Figure 6(c) shows the plots of radiation efficiency magnitude for three proposed designs of H-SRR antenna. The radiation efficiency at 2.4/5.2 GHz is found to be 96%/93% for design 1, 96%/94% for design 2, and 96%/93% for design 3.

3. IMPEDANCE MODELING OF H-SRR ANTENNA

From return loss characteristics in Figures 3(a), (e), it is observed that the proposed H-SRR antenna with metallic loadings acts as a bandpass filter at frequencies under study, i.e., 2.4/5.2 GHz. The analytical

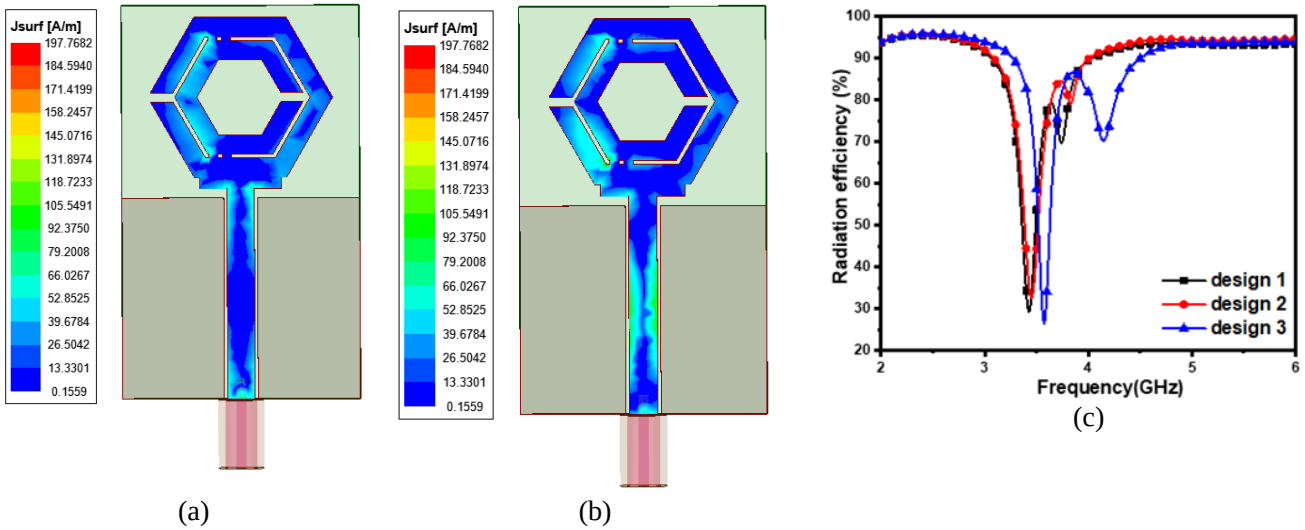

Figure 6. The surface current distribution of H-SRR (design 3) at (a) 2.4 GHz and (b) 5.2 GHz, (c) radiation efficiency plot.

modeling was reported earlier to calculate the resonant frequency of the H-SRR structure [27], which is unable to incorporate the role of a feed line as well as any modifications such as metallic loading in this structure. An impedance modeling based on return loss measurements is reported to address such issues [21], which also helped to understand the inductive effect of the metallic loading in achieving the desired frequencies as well as a wider bandwidth. In the same way, the input impedance Z_{in} (or admittance Y_{in}) value is obtained from the simulated/measured return loss data of the H-SRR antenna and using the set of Equations (5)–(7) for input admittance (Y_{in}) derived from the impedance equivalent circuit of the H-SRR structure as shown in Figure 7.

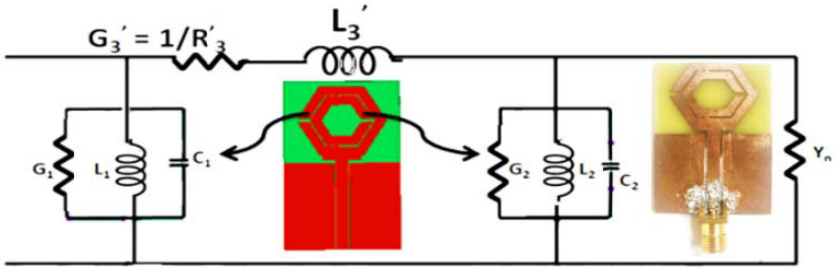

Figure 7. Equivalent impedance circuit of the H-SRR antenna (#design 3).

In Figure 7, L_1, C_1, G_1 are lumped parameters for the outer ring of the radius R_1 in an H-SRR antenna (Figure 1); L_2, C_2, G_2 are for the inner ring of the radius R_2; G'_3, L'_3 represent the total conductance and inductance for the four metallic loadings (S_1, S_2, S_3, S_4) connecting both the rings of the H-SRR structure (design 3). Y_n is the intrinsic admittance of the free space. Here, $G'_3 = G_3 + G_4$ and $L'_3 = L_3L_4/(L_3 + L_4)$, G_3 and L_3 are the conductance and inductance for the two metallic loadings (S_1, S_3), and G_4, L_4 are the conductance and inductance for the other two metallic loadings (S_2, S_4). The expression for overall input admittance is [21],

$$Y_{in} = G_1G_2 + G_1G'_3 + G'_3G_2 + \frac{(1-\omega^2L_2C_2)}{j\omega L_2}\left(G_1 + G'_3\right) + \frac{(1-\omega^2L_1C_1)}{j\omega L_1}\left(G_2 + G'_3\right) - \left[\frac{(1-\omega^2L_1C_1)}{\omega^2L_1L'_3} + \frac{(1-\omega^2L_2C_2)}{\omega^2L_1L_2}\right] - \left[\frac{(1-\omega^2L_1C_1)(1-\omega^2L_2C_2)}{\omega^2L_1L_2}\right] + Y_n \quad (5)$$

Since $Y_{in} = G_{in} + jB_{in}$ where G_{in} is the input conductance and B_{in} is the input susceptance of the H-SRR antenna, we get the following expressions by comparing the real and imaginary parts with Equation (5) [21]

$$G_{in} = G_1G_2 + G_1G_3' + G_3'G_2 - \left[\frac{(1-\omega^2L_1C_1)}{\omega^2L_1L_3'} + \frac{(1-\omega^2L_2C_2)}{\omega^2L_1L_2}\right] - \left[\frac{\left(1-\omega^2L_1C_1\right)(1-\omega^2L_2C_2)}{\omega^2L_1L_2}\right] \quad (6)$$

$$B_{in} = \frac{(1-\omega^2L_2C_2)}{j\omega L_2}\left(G_1+G_3'\right) + \frac{(1-\omega^2L_1C_1)}{j\omega L_1}\left(G_2+G_3'\right) \quad (7)$$

Equations (5)–(7) are used to calculate all lumped parameters shown in Figure 7 from the simulated/measured return loss values of H-SRR and C-SRR antennas. Table 4 shows the calculated values of these lumped parameters for three simulated H-SRR designs, fabricated C-SRR, and H-SRR antennas. The lumped element values of L_1, C_1, L_2, and C_2 are found to be almost the same except for design 2. Thinner metallic loadings for design 1 give the highest L_3' as well as G_3', and the introduction of wider loadings as in design 2 or one more set of metallic loadings in design 3 led to lower values of these parameters. Further, lower values of L_3' and G_3' of the fabricated H-SRR antenna have contributed to widening the bandwidth (BW) as compared to the fabricated C-SRR antenna. The performances of the H-SRR antenna with metallic loadings are summarized in Table 5 along with the previously published work. From Table 5, it can be seen that the proposed H-SRR antenna provides a dual-band response with wider impedance bandwidth of 27.67%/74.50% and better gain at 2.4/5.2 GHz bands, respectively, compared to earlier reported antennas [15, 18, 20, 21]. By using 3 or 4 H-SRR on the top layer with a slotted ground layer or as a coupling structure, more than two times higher gain or 100% bandwidth is reported [30–32] than the proposed H-SRR antenna, which still maintains the simplicity in design. Thus, the H-SRR antenna can be used to transmit more channels in the 2.4/5.2 GHz bands. The calculated Q factor for C-SRR is found to be 6.27/4.57 at 2.4/5.2 GHz, and for H-SRR, it is 3.53/1.31 at 2.4/5.2 GHz, respectively. Thus, the use of optimized four-metallic loadings helps in achieving a wider band and comparatively higher gain for proposed H-SRR antennas.

Table 4. The calculated values of lumped parameters for simulated and fabricated antennas.

Parameters	**design 1**	**design 2**	**design 3**	**Fabricated C-SRR prototype**	**Fabricated H-SRR prototype**
L_1 (nH)	17.06	20.15	18.34	19.14	18.93
C_1 (μF)	0.2	0.19	0.22	0.227 (pF)	0.23
L_2 (nH)	83.98	24.43	81.81	11.79	17.32
C_2 (fF)	0.11	0.38	0.11	78.63	0.52
L_3' (pH)	191	8.67	61	3.08×10^3	94.5
G_3' (S)	5.5	1.00	1.00	0.99	2.00

4. SPACE DIVERSITY PERFORMANCE OF H-SRR ANTENNA

The space diversity performance of the H-SRR antenna is investigated in terms of receiver diversity in the single input-multiple output (SIMO) system and transmitter diversity in the multiple-input-single-output (MISO) system.

4.1. Receiver Diversity and Channel Capacity of SIMO System

For the receiver diversity, one H-SRR antenna acting as a transmitting (Tx) antenna is kept at position 1, and three receiving (Rx) antennas, one H-SRR, and two C-SRR antennas are kept at three different positions (2, 3, 4) concerning position 1. Also, the receiver antennas are placed in two arrangements individually, i.e., the linear and spherical arrangements for the SIMO system output of 1Tx × 3Rx.

Table 5. Comparison between the present work and other reference antennas.

Shape of Antenna/Reference	ε_r of the substrate	Frequency (GHz)	Electrical Size of the antenna	IBW (in %)	Gain (dB)	Design complexity
Semi-elliptical patch [15]	4.4 (FR-4)	2.4–12	$0.16\lambda \times 0.12\lambda$	–	0.2	Complex
Rectangular-SRR [18]	6.15 (Roger)	2.4, 5.2, 5.8	$0.32\lambda \times 0.208\lambda$	10, 58	−2, 4	Most Simple
Circular-SRR [20]	4.4 (FR-4)	2.4, 5.2	$0.344\lambda \times 0.208\lambda$	27.50, 70.58	2.14, 0.34	Most Simple
Circular-SRR [21]	4.4 (FR-4)	2.4, 5.2	$0.344\lambda \times 0.208\lambda$	30, 70.78	2.11, 0.36	Most Simple
H-SRR [30]	4.3 (FR-4)	3	$0.23\lambda \times 0.19\lambda$	146.91	3.88	Complex
H-SRR [31]	4.4 (FR-4)	8.52, 11.38	$0.71\lambda \times 0.88\lambda$	28.40, 10.19	4.63, 4.01	Complex
H-SRR [32]	4.3 (FR-4)	5.98	$0.526\lambda \times 0.518\lambda$	72.5	5.97	Complex
Our work						
H-SRR (design 1)	**4.4 (FR-4)**	**2.4, 5.2**	$0.344\lambda \times 0.208\lambda$	**24.34, 72.62**	**2.24, 1.46**	**Simple**
H-SRR (design 2)	**4.4 (FR-4)**	**2.4, 5.2**	$0.344\lambda \times 0.208\lambda$	**23.90, 74.42**	**2.32, 1.11**	**Simple**
H-SRR (design 3)	**4.4 (FR-4)**	**2.4, 5.2**	$0.344\lambda \times 0.208\lambda$	**27.67, 74.50**	**2.31, 1.26**	**Simple**
Fabricated H-SRR	**4.4 (FR-4)**	**2.4, 5.2**	$0.344\lambda \times 0.208\lambda$	**50, 76.53**	**2.32, 2.57**	**Simple**

where λ is the free space wavelength at the lower operating band.

Table 6. Different cases for the receiver diversity of antenna.

CASES	POSITION 1 (Transmitting antenna)	POSITION 2 (Receiving antenna)	POSITION 3 (Receiving antenna)	POSITION 4 (Receiving antenna)
1.	H-SRR	H-SRR	C-SRR	C-SRR
2.	H-SRR	H-SRR	C-SRR	–
3.	H-SRR	H-SRR	–	–

Table 6 shows cases 1, 2, and 3 based on different placements of H-SRR and C-SRR antennas at positions 1, 2, 3, and 4, respectively. For instance, in case 1, the transmitting antenna is H-SRR antenna kept at a fixed position from three receiving antennas as H-SRR, C-SRR, and C-SRR antennas, placed respectively at three different positions. The distance between position 2 and position 1 is kept at 32 cm; for positions 3, and 4, it is 34 cm from position 1 in the linear arrangement of antennas; in the case of a spherical arrangement, the positions 2, 3, and 4 are at a radial distance of 30 cm, each from position 1, i.e., transmitting antenna.

Figures 8(a)–(f) show the antenna arrangements for various cases with different views along with a power divider at the receiver end in the anechoic chamber. The foams of low dielectric constant 1.6 are used to place the SRR antennas. The received power (P_r), carrier-to-noise ratio (C/N), and carrier-to-noise-density ratio (C/No) values are obtained with the input power variation in the range of 0 to 20 dBm for all three cases in both linear and spherical arrangements of receiver antennas at 2.4/5.2 GHz. Such arrangements form an array of the receiving antennas, so the array factor also contributes to the total receiving power. The power divider used in the measurement is COMPEL PD0981-4W which is an RF broadband, 4-way, power divider, and power combiner furnished with SMA female connectors and featured with 2 dB max. insertion loss and 14 dB min. isolation. The measured insertion loss ($-S_{21}$) of the power divider is about −0.79 dB and −7.75 dB at 2.4 GHz and 5.2 GHz frequencies, respectively.

Figures 9(a)–(d) show the plot of received power vs. incident power, and it is observed that the net received power increases almost linearly with the incident power, while it decreases as the number of receiving antennas decreases subsequently. In linear arrangements, the received power P_r is found in the range of −64 dBm to −45 dBm at 2.4 GHz for case 1 when all three Rx antennas are in use, and it is lowered to −52 dBm at 5.2 GHz for the input power of 20 dBm for case 1. Also, for 2.4 GHz, only a slight variation in P_r values is observed among the three cases as in Figure 9(a), while the variation is large at 5.2 GHz as shown in Figure 9(b), indicating that the larger diversity effect is at higher frequency

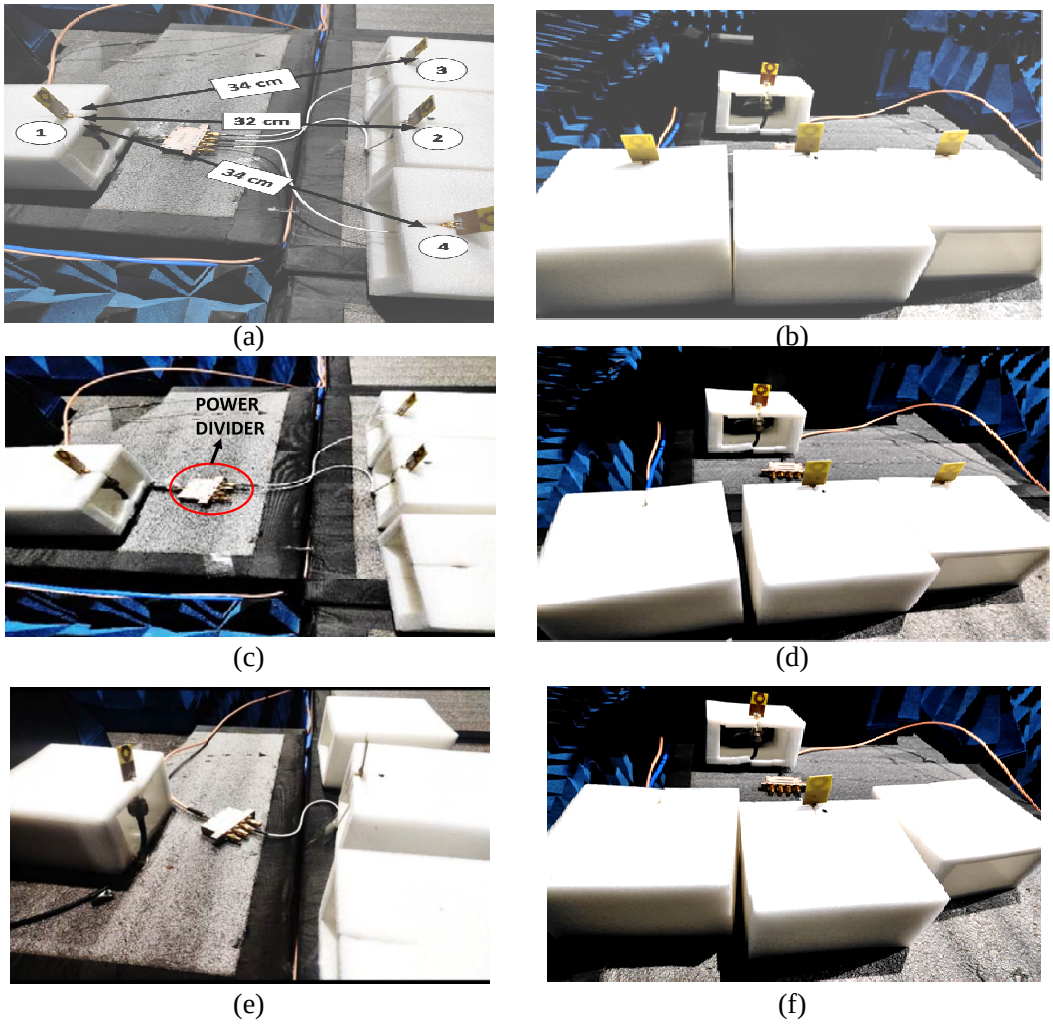

Figure 8. Measurement set up to investigate the receive diversity using H-SRR and C-SRR antennas in SIMO systems. (a) Case 1 (Side view). (b) Case 1 (Front view). (c) Case 2 (Side view). (d) Case 2 (Front view). (e) Case 3 (Side view). (f) Case 3 (Front view).

in the linear arrangement. In cases 1 and 3 at 2.4 GHz in Figure 9(c), the same P_r range as in linear arrangements indicates more dependency on the number of antennas for spherical arrangement.

However, at 5.2 GHz, a lower P_r is observed in the spherical arrangements, especially for cases 2 and 3 in the far-field region. This confirms that space diversity using H-SRR antennas is more dependent on position arrangement and operating frequency rather than the number of antennas.

In Figures 10(a)–(d), the measured C/N with incident power shows that as the magnitude of the incident power is increased from 0 dBm to 20 dBm, the C/N ratio is found to linearly rise from 31 dBc to 48 dBc at 2.4 GHz for case 1, while it is 2 to 3 dBc lower for cases 2 and 3, due to lesser number of Rx antennas in the linear arrangement, and indicates lower reception of the desired 2.4 GHz signal. A similar range of C/N is noted in spherical arrangements at 2.4 GHz as in Figure 10(c) and at 5.2 GHz, and lower C/N is found in the range of 24 dBc to 36 dBc with larger variation with the input power for each case in Figure 10(b) and Figure 10(d). This confirms larger crosstalk between antennas at a higher frequency, which lowers net received power as well as creates fading in the reception.

Figures 11(a)–(d) show the measured carrier-to-peak-noise density ratio (C/No) in dBc/Hz in a linear relationship with the input power which is found to be slightly dependent on the number of antennas. The C/No is in the range of 74 dBc/Hz to 88 dBc/Hz for case 1, i.e., three Rx antennas at 2.4 GHz in the linear arrangement, and then it decreases with one or two Rx antennas as in Figure 11(a).

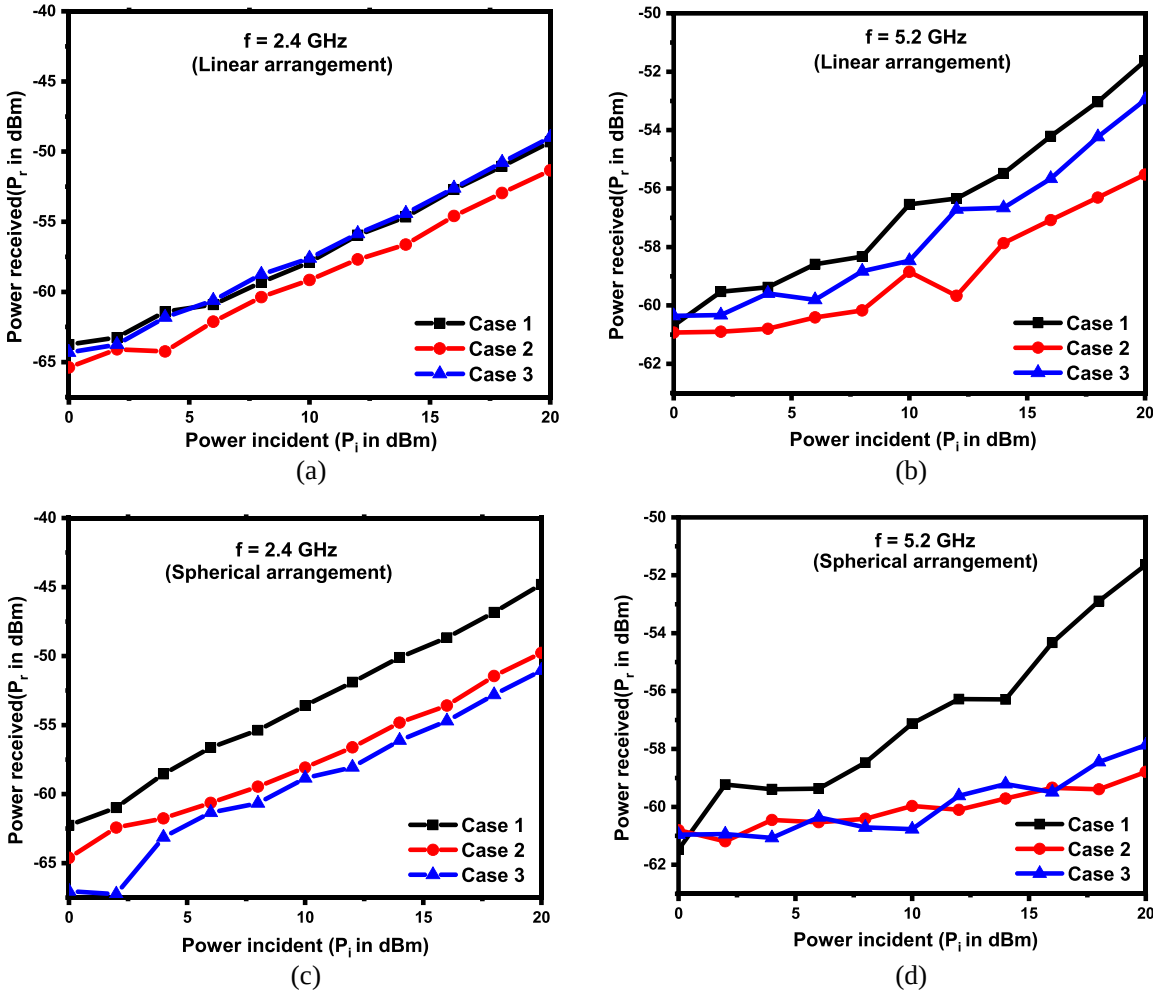

Figure 9. Measured received power variation with incident power for various cases of SIMO system. (a) Linear arrangement at 2.4 GHz, (b) linear arrangement at 5.2 GHz, (c) spherical arrangement at 2.4 GHz, and (d) spherical arrangement at 5.2 GHz.

Other C/No performances are similar to C/N performances for all cases 1, 2, and 3 at 2.4/5.2 GHz in both arrangements. The channel capacity (CC) of the SIMO system is given in Equation (8) as [7]

$$\mathrm{CC} = M_r B \mathrm{Log}_2\left(1 + \frac{C}{N}\right) \tag{8}$$

where B is the bandwidth of the signal, C/N the carrier-to-noise ratio, and M_r the number of Rx antennas. For cases 1, 2, and 3, the value of M_r is 3, 2, and 1, respectively, as shown in Figures 8(a), (c), (e). The bandwidth in measurement is kept at 10 kHz in the spectrum analyzer R&S FSL6. Using Equation (8), the calculated channel capacity (in Mbps) is shown in Figures 12(a)–(b) for all cases 1 to 3 in linear and spherical SIMO (1Tx × 3 Rx) systems. The CC of case 1-based SIMO system using the H-SRR and C-SRR antennas is obtained in the range of (2.70–3.75) Mbps at 2.4 GHz and (2.70–3.50) Mbps at 5.2 GHz, respectively, in the linear arrangement, while it is (3.0–4.50) Mbps at 2.4 GHz and (2.90–3.50) Mbps at 5.2 GHz in the spherical arrangement. Also, the rate of increase is a little higher at the lower band, i.e., 2.4 GHz with the applied input power (in dBm) for the same bandwidth of 10 kHz; however, for the same percentage bandwidth, a 5.2 GHz band supports almost twice the CC of that at 2.4 GHz band. The CC values are found to be almost the same in both linear and spherical arrangements for cases 2 and 3 and increase with the number of Rx antennas rather than the input power range.

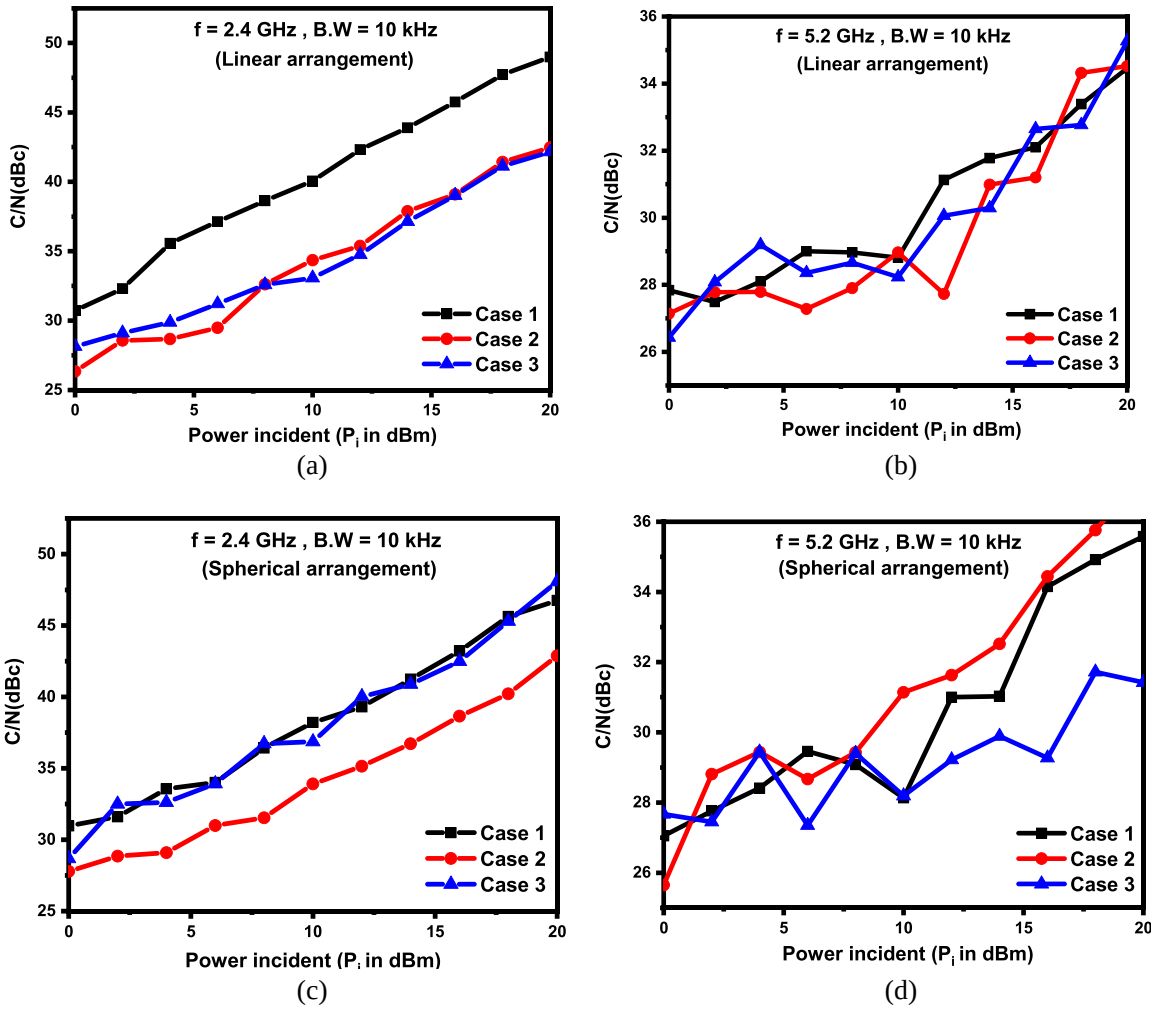

Figure 10. Measured C/N variation with incident power for various cases of SIMO system, (a) linear arrangement at 2.4 GHz, (b) linear arrangement at 5.2 GHz, (c) spherical arrangement at 2.4 GHz, and (d) spherical arrangement at 5.2 GHz.

4.2. Transmitter Diversity and Channel Capacity of MISO System

For transmitter diversity, one H-SRR antenna acting as a receiving (Rx) antenna is kept at position 1, and three transmitting (Tx) antennas, one H-SRR, and two C-SRR antennas are kept at three different positions (2, 3, 4), i.e., the linear and spherical MISO arrangements as 3Tx × 1Rx antennas at 2.4/5.2 GHz. Table 7 shows all cases based on different placements of H-SRR and C-SRR antennas at positions 1, 2, 3, and 4, respectively.

Table 7. Different cases for the transmitter diversity of antenna.

CASES	POSITION 1 (Receiving antenna)	POSITION 2 (Transmitting antenna)	POSITION 3 (Transmitting antenna)	POSITION 4 (Transmitting antenna)
1.	H-SRR	H-SRR	C-SRR	C-SRR
2.	H-SRR	H-SRR	C-SRR	–
3.	H-SRR	H-SRR	–	–

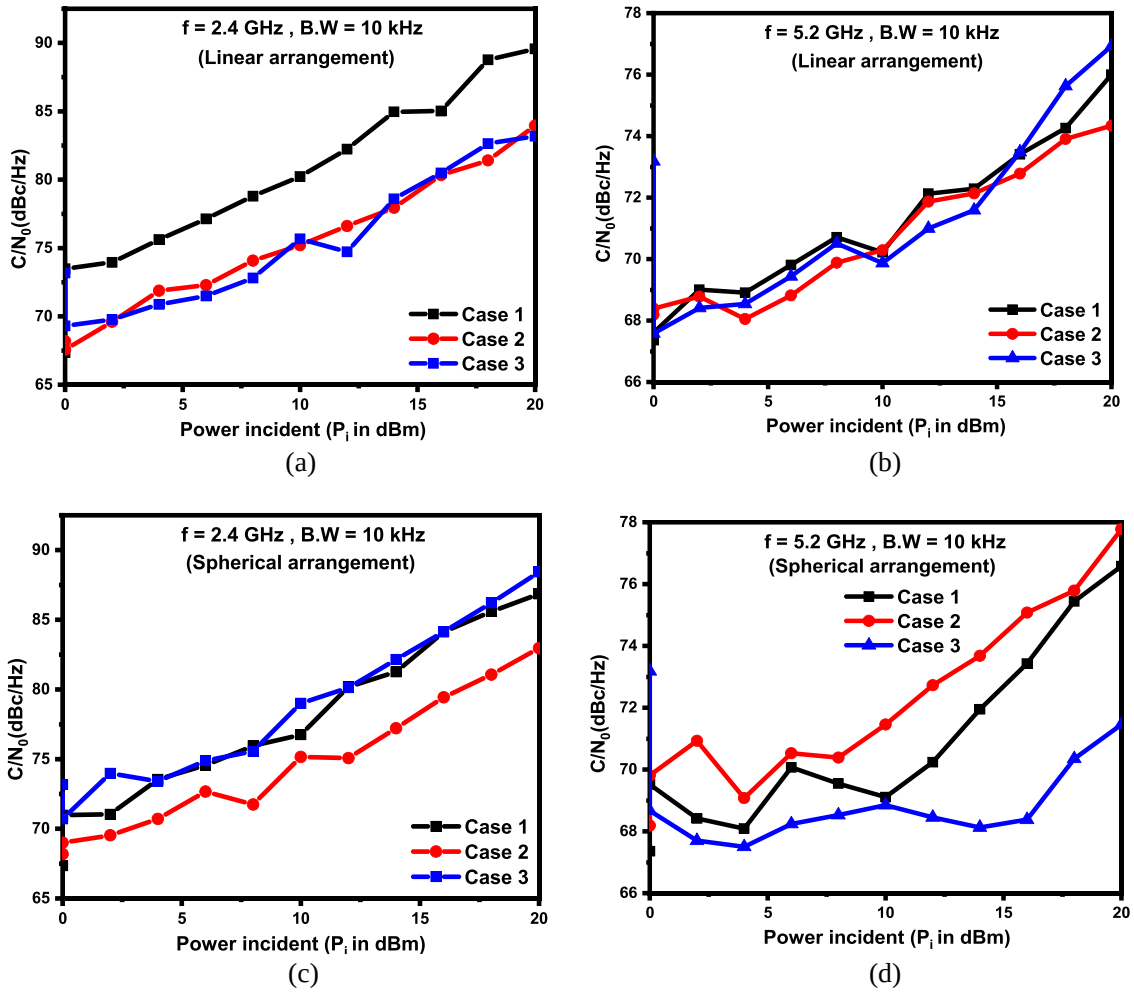

Figure 11. Measured carrier-to-noise power density (C/No) variation with incident power for various cases of SIMO system, (a) linear arrangement at 2.4 GHz, (b) linear arrangement at 5.2 GHz, (c) spherical arrangement at 2.4 GHz, and (d) spherical arrangement at 5.2 GHz.

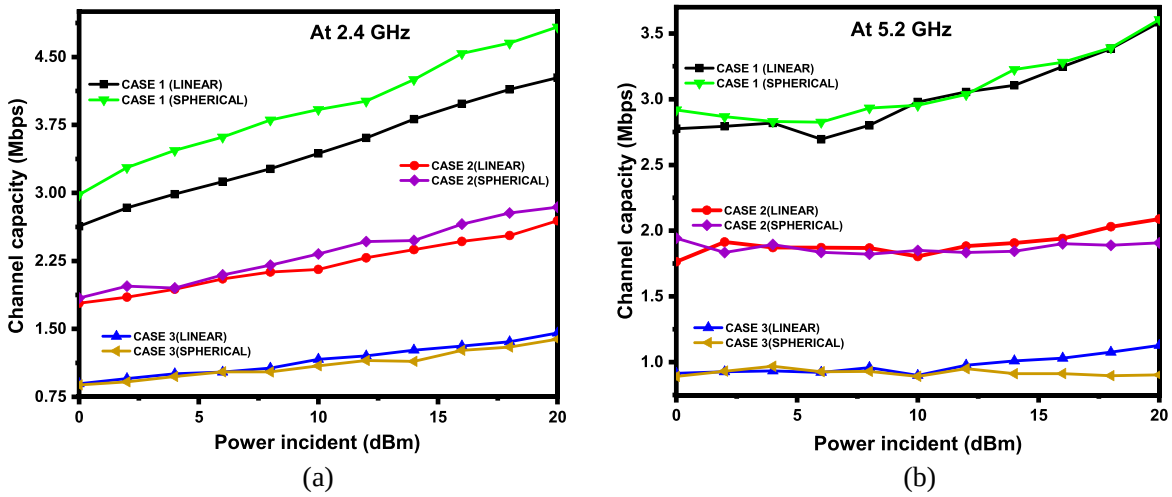

Figure 12. Calculated channel capacity of various cases in SIMO system at two frequencies, (a) 2.4 GHz, and (b) 5.2 GHz.

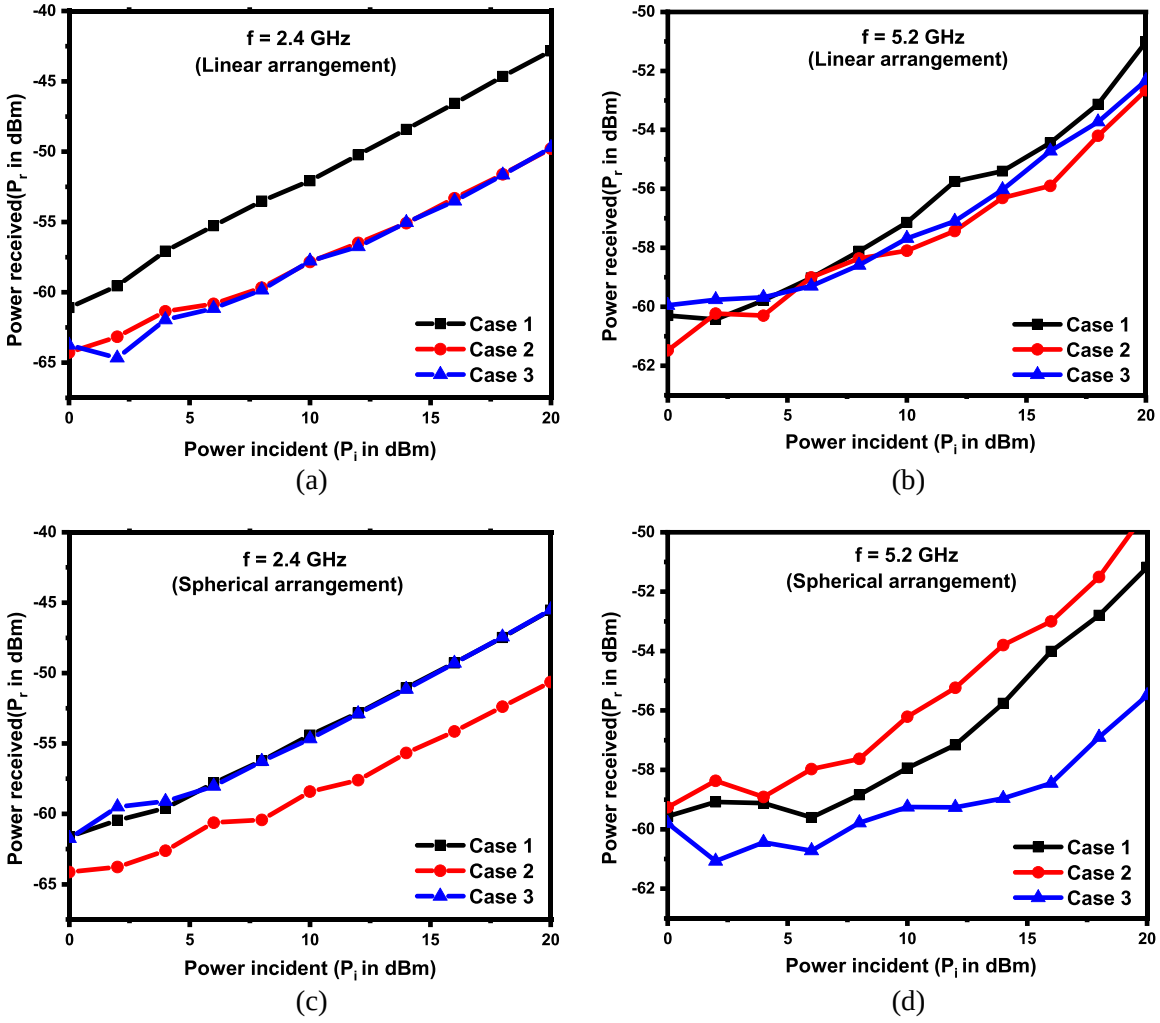

Figure 13. Measured received power variation with incident power for various cases of MISO system, (a) linear arrangement at 2.4 GHz, (b) linear arrangement at 5.2 GHz, (c) spherical arrangement at 2.4 GHz, and (d) spherical arrangement at 5.2 GHz.

Figures 13(a)–(d) show the plot of received power vs incident power in the range of 0 to 20 dBm. In the linear arrangement shown in Figure 13(a), the received power is found in the range of −58 to −43 dBm at 2.4 GHz for case 1, when all three Tx antennas are in use, while it reaches −51 dBm at 5.2 GHz for the input power of 20 dBm for the same case in Figure 13(b). In cases 1 and 2 at 2.4 GHz for the spherical arrangement as in Figures 13(c)–(d). Slightly lower P_r is obtained than that in linear arrangements, and it is about 4–5 dBm higher in case 3. These results again confirm that the transmitter diversity too is mainly dependent on the position arrangement, i.e., space diversity of the antennas and frequency. Figures 14(a)–(d) show that as the incident power is increased from 0 dBm to 20 dBm, the C/N ratio is found to linearly rise from 31 dBc to 48 dBc at 2.4 GHz for case 1, while it is 6 to 7 dBc lower for cases 2 and 3, due to less Tx antennas in a linear arrangement. A slightly lower range of C/N is noted at 5.2 GHz as in Figure 14(b) and found to be in the same range of 26 dBc to 35 dBc for all three cases. In the spherical arrangements at 2.4 GHz as in Figure 14(c) and at 5.2 GHz as in Figure 14(d), a similar range of the C/N is found as in the linear arrangements.

However, the variations in C/N values at 5.2 GHz indicate large mutual interference of signals at the higher frequency, which becomes larger with the high input power of 20 dBm. The variations in C/No performances are found to be similar for cases 1, 2, and 3 at 2.4/5.2 GHz in both arrangements as that of C/N performances. In the present MISO (3Tx × 1Rx) setup of measurement, the number of

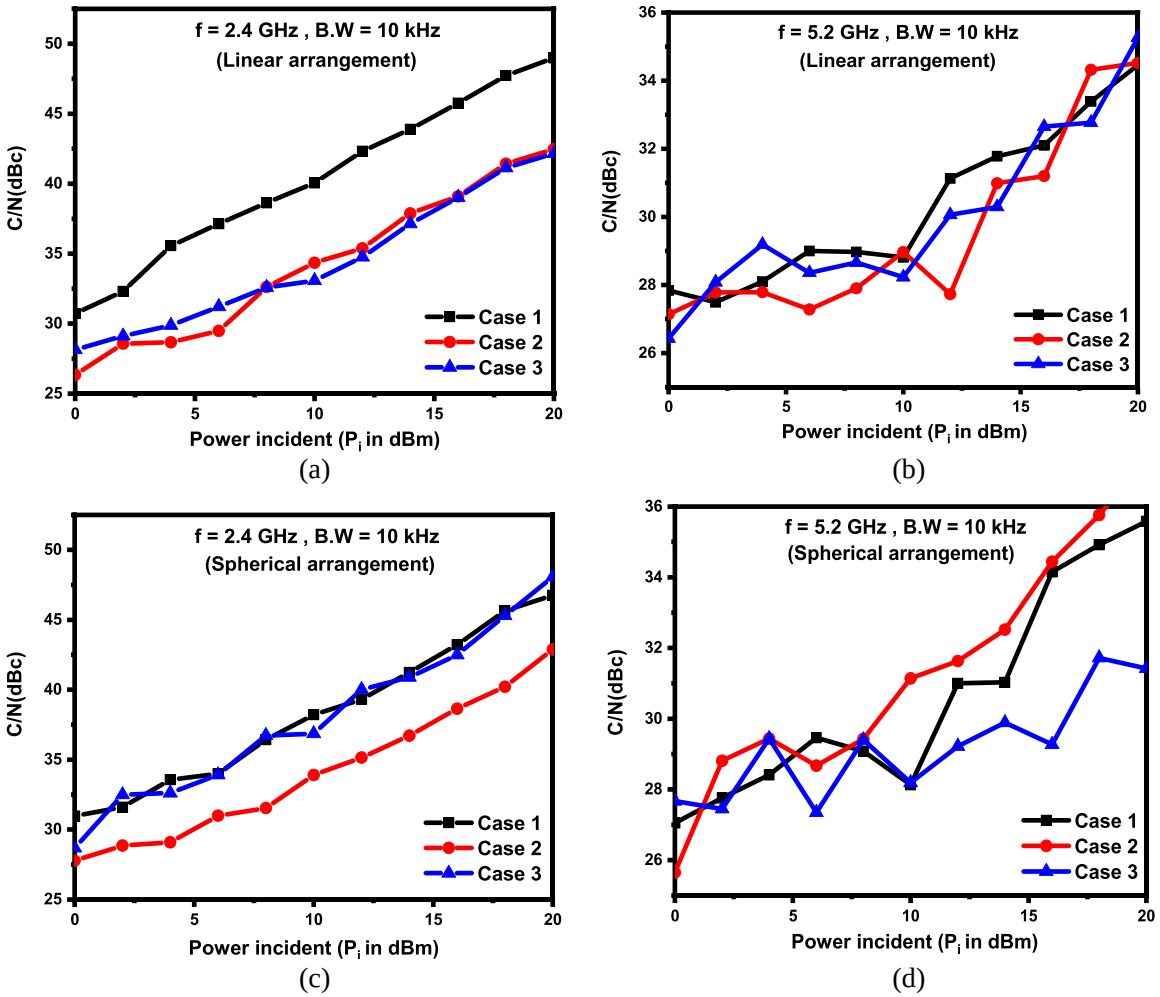

Figure 14. Measured C/N variation with incident power for various cases of MISO system at two frequencies, (a) linear arrangement at 2.4 GHz, (b) linear arrangement at 5.2 GHz, (c) spherical arrangement at 2.4 GHz, and (d) spherical arrangement at 5.2 GHz.

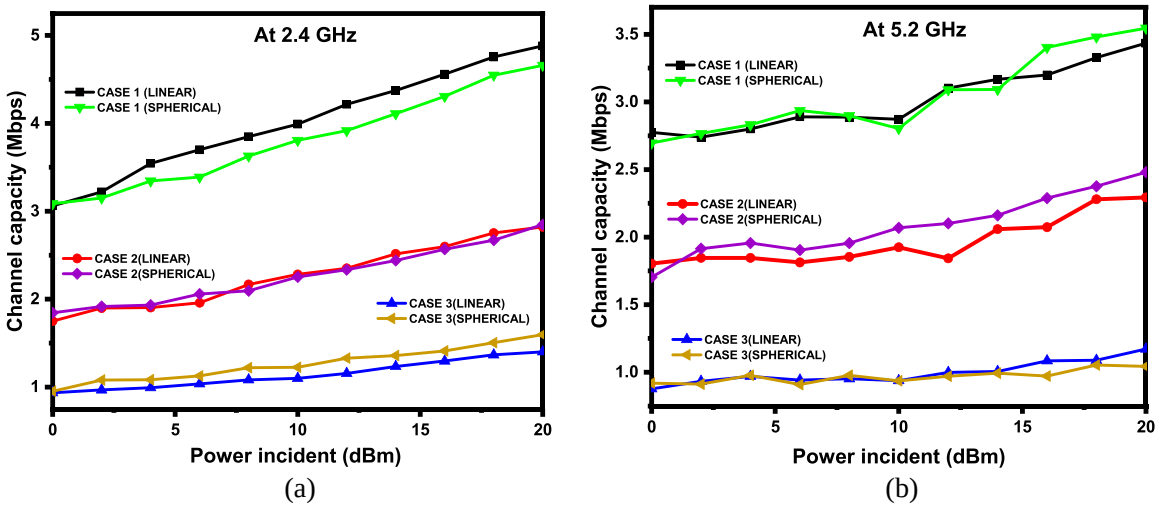

Figure 15. Calculated channel capacity of various cases in the MISO system at two frequencies, (a) 2.4 GHz, and (b) 5.2 GHz.

antennas used at the transmitter end is taken as $M_t = 3, 2, 1$ for cases 1, 2, and 3, respectively, and the bandwidth is kept the same as 10 kHz in Equation (8). The calculated CC (in Mbps) is shown in Figures 15(a)–(b) for all cases. The CC of SIMO and MISO configurations with the existing antennas can be compared in Table 8.

Table 8. Channel capacity for different diversity cases for the receiver diversity of antenna.

Space diversity	CC (in Mbps) in linear arrangement	CC (in Mbps) in spherical arrangement
Receiver diversity (SIMO) Case 1	(2.70–3.75) @ 2.4 GHz (3.00–4.50) @ 5.2 GHz	(2.70–3.50) @ 2.4 GHz (2.90–3.50) @ 5.2 GHz
Transmitter diversity (MISO) Case 1	(3.10–4.80) @ 2.4 GHz (3.20–4.50) @ 5.2 GHz	(2.80–3.50) @ 2.4 GHz (2.75–3.50) @ 5.2 GHz

As can be seen in Figure 16 and Table 8, the CC of the MISO system is found to be independent of antenna position and dependent on the number of antennas similar to receiver diversity (SIMO). Thus, the proposed H-SRR antennas are useful for high-speed transmission in MISO communication systems like multi-path channel transmission [33].

5. CONCLUSION

A dual-band H-SRR antenna with metallic loadings is proposed for the WLAN/WiMAX applications according to the IEEE 802.11 a/b standards. The transmitter and receiver diversities are studied with the H-SRR antenna and additional two C-SRR antennas at 2.4/5.2 GHz bands for SIMO and MISO systems. The carrier-to-noise ratio (C/N) and carrier-to-noise-density ratio (C/No) values are found to increase with the number of antennas and vary linearly in the linear arrangements of receiving/transmitting antennas in SIMO/MISO systems, whereas the slightly nonlinear increase in these parameters is observed for the spherical arrangements of the same antennas. The calculated channel capacity (CC) shows that it is dependent more on the number of antennas than on the placement of antennas. Thus, the reported H-SRR antennas are suitable for employment in both systems for space diversity performance.

ACKNOWLEDGMENT

The authors thank the Department of Electronic Science, South Campus, University of Delhi, and Atma RamSanatan Dharma College, University of Delhi, for providing the necessary support and infrastructure for carrying out this work. The authors would like to thank the Faculty Research Programme (FRP) of the Institute of Eminence (IoE) system of the University of Delhi (Letter Ref./No./IoE/2021/12/FRP dated 29.10.2021).

REFERENCES

1. Shah, C. R., "Performance and comparative analysis of SISO, SIMO, MISO and MIMO," *International Journal of Wirel. Commun. Simul.*, Vol. 9, No. 1, 1–4, 2017.
2. Alrubei, M. A. T., I. A. Alshimaysawe, A. N. Hassan, and A. H. K. Khwayyir, "Capacity analysis and performance comparison of SISO, SIMO, MISO & MIMO systems," *Journal of Physics Conference Series*, Vol. 1530, No. 1, 12077, 2020.
3. Bialkowski, M. E., "Research into multiple-element antennas to enhance performance of wireless communication systems," *International Conference on Microwaves, Radar & Wireless Communications*, 1071–1082, 2006.

4. Zhang, H. and H. Dai, "On the capacity of distributed MIMO systems," *Conference on Information Sciences and Systems*, 1–5, Princeton University, 2004.
5. Shr, K. T., H. D. Chen, Y. and H. Huang, "A low-complexity Viterbi decoder for space-time trellis code," *IEEE Transactions on Circuits and Systems I: Regular Papers*, Vol. 57, No. 4, 873–885, 2010.
6. Ghayoula, E., A. Bouallegue, and R. Ghayoula, "Capacity and performance of MIMO systems for wireless communications," *Journal of Engineering Science and Technology Review*, Vol. 7, No. 3, 108–111, 2014.
7. Sengar, K., N. Rani, A. Singhal, et al., "Study and capacity evaluation of SISO, MISO and MIMO RF wireless communication systems," *International Journal of Engineering Trends and Technology*, Vol. 9, No. 9, 436–440, 2014.
8. Giri, N. C., A. Sahoo, and J. R. Swain, "Capacity & performance comparison of SISO and MIMO system for next-generation network (NGN)," *International Journal of Advanced Research in Computer Engineering & Technology*, Vol. 3, No. 9, 30131–33035, 2014.
9. Janaswamy, R., *Radio Wave Propagation and Smart Antennas for Wireless Communications*, 1st Edition, Springer Science & Business Media, 2001.
10. Available at: https://www.comm.utoronto.ca/∼rsadve/Notes/DiversityReceive.pdf.
11. Verdu, S., *Multiuser Detection*, Cambridge University Press, 1998.
12. Available at: https://www.analogictips.com/signal-channel-diversity-fading-part-1-space-diversity/.
13. Godara, L. C., *Handbook of Antennas in Wireless Communications*, CRC Press, 2018.
14. Eldek, A., "Numerical analysis of a small ultra wideband microstrip-fed tap monopole antenna," *Progress In Electromagnetics Research*, Vol. 65, 59–69, 2006.
15. Benkhadda, O., S. Ahmad, M. Saih, et al., "Compact broadband antenna with Vicsek fractal slots for WLAN and WiMAX applications," *Applied Sciences*, Vol. 12, No. 3, 1142, 2022.
16. Yamac, Y. E. and S. C. Basaran, "A compact dual-band implantable antenna based on split-ring resonators with meander line slots," *22nd International Conference on Applied Electromagnetics and Communications*, 1–3, 2016.
17. Zaker, R., C. Ghobadi, and J. Nourinia, "A modified microstrip-fed two-step tapered monopole antenna for UWB and WLAN applications," *Progress In Electromagnetics Research*, Vol. 77, 137–148, 2007.
18. Basaran, S. C. and K. Sertel, "Dual wideband CPW-fed monopole antenna with split-ring resonators," *Microwave and Optical Technology Letters*, Vol. 55, No. 9, 2088–2092, 2013.
19. Gabriel, S., R. W. Lau, and C. Gabriel, "The dielectric properties of biological tissues: III. Parametric models for the dielectric spectrum of tissues," *Physics in Medicine and Biology*, Vol. 41, No. 11, 2271–2293, 1996.
20. Sehgal, P. and K. Patel, "Dual-wideband CPW-fed monopole antenna with circular split-ring resonators," *7th International Conference on Signal and Integrated Networks*, 1078–1083, 2020.
21. Sehgal, P. and K. Patel, "Performance analysis and impedance modeling of rectangular and circular split-ring resonator antennas in 2.4/5.2 GHz bands," *Progress In Electromagnetics Research C*, Vol. 117, 159–171, 2022.
22. Jagadish, M. and A. S. Pradeep, "Design of hexagonal-shaped split ring resonator for multi-resonant behaviour," *Bonfring International Journal of Research in Communication Engineering*, Vol. 6, 20–23, 2016.
23. Singh, A. and S. K. Sharma, "Calculation of resonant frequency of hexagonal split ring resonator using ANN," *International Journal of Research in Engineering and Technology*, Vol. 3, 144–147, 2014.
24. Rajni, M. A., "An accurate approach of mathematical modeling of SRR and SR for metamaterials," *Journal of Engineering Science and Technology Review*, Vol. 9, 82–86, 2016.

25. Daniel, R. S., R. Pandeeswari, and S. Raghavan, "A miniaturized printed monopole antenna loaded with hexagonal complementary split-ring resonators for multiband operations," *International Journal of RF and Microwave Computer-Aided Engineering*, Vol. 28, No. 7, 21401, 2018.
26. Min, H., J. Lee, and S. Park, "Capacity enhancement using an interference-limited area for device-to-device uplink underlaying cellular networks," *IEEE Transactions on Wireless Communications*, Vol. 10, No. 12, 3995–4000, 2011.
27. Marques, R., F. Mesa, and J. Martel, "Comparative analysis of edge and broadside-coupled split ring resonators for metamaterial design — Theory and experiments," *IEEE Transactions on Antennas and Propagation*, Vol. 51, No. 10, 2572–2581, 2003.
28. Cole, H., Z. Hu, and Y. Wang, "Operating range evaluation of RFID system," *Advanced Radio Frequency Identification Design and Applications, Stevan Preradovic*, 1–28, InTech, 2011.
29. Kaushal, V., A. Birwal, and K. Patel, "Path loss of two-port circular-ring slot antenna for RFID applications," *IEEE International Conference on RFID Technology and Applications (RFID-TA)*, 120–123, Delhi, 2021.
30. Islam, M. T., F. B. Ashraf, T. Alam, et al., "A compact ultrawideband antenna based on hexagonal split-ring resonator for pH sensor application," *Sensors*, Vol. 18, No. 9, 2959, 2018.
31. Swetha, A. and M. Vanidivyatha, "CPW fed antenna inspired by a broad side coupled hexagonal SRR for X-band applications," *Proceedings of Advances in Decision Sciences, Image Processing, Security and Computer Vision International Conference on Emerging Trends in Engineering (ICETE)*, Vol. 2, 52–60, 2019.
32. Saktioto, Y. Soerbakti, R. F. Syahputra, et al., "Improvement of low-profile microstrip antenna performance by hexagonal-shaped SRR structure with DNG metamaterial characteristic as UWB application," *Alexandria Engineering Journal*, Vol. 61, No. 6, 2022.
33. Naik, K. K., T. V. Ramakrishna, and T. L. Charan, "Design a tri-band hexagonal patch antenna for wireless applications," *Energy Systems, Drives and Automations*, 659–667, 2020.